II International Conference on Particle-based Methods - Fundamentals and Applications
PARTICLES 2011
E. Oñate and D.R.J. Owen (Eds)

A TANGENTIAL FORCE-DISPLACEMENT MODEL FOR ELASTIC FRICTIONAL CONTACT BETWEEN PARTICLES IN TRIAXIAL TEST SIMULATIONS

PIETER FRANKEN*, STIJN FRANÇOIS*, ENGELBERT TIJSKENS† AND GEERT DEGRANDE*

*Department of Civil Engineering, K.U.Leuven
Kasteelpark Arenberg 40, B-3001 Leuven, Belgium
web page: http://bwk.kuleuven.be/bwm
e-mail: Pieter.Franken@bwk.kuleuven.be

†Department of Biosystems, K.U.Leuven
Kasteelpark Arenberg 30, B-3001 Leuven, Belgium

Key words: Discrete Element Method, Triaxial Test, Tangential Contact Model, Granular Soil

Abstract. A tangential contact model for three-dimensional discrete element simulations is proposed and used in the micro-mechanical simulation of a drained triaxial test. In this model, the dependence of the tangential contact force on the contact loading history is accounted for. A representative volume element with spherical discrete elements and periodic boundary conditions is used in the simulations to reduce the computation costs. Numerical results of a triaxial test obtained with a linear and the proposed tangential contact model are compared. The results for both contact models are qualitatively in agreement with theory. The linear contact model needs calibration as the used parameters lack physical meaning, while the proposed contact model only uses physical properties of the particles.

1 INTRODUCTION

A phenomenological approach, where parameters are used to describe the behaviour observed in physical tests, such as triaxial tests, is frequently used to study the behaviour of granular soils. When studying accumulation phenomena in granular soils resulting from repeated small amplitude dynamic loading, however, phenomenological models exhibit limitations. Current accumulation models [7, 13] use a large number of parameters that often lack physical meaning. As a result, little insight in the physical processes is gained, while an extensive amount of laboratory tests has to be performed for model calibration.

As an alternative, a micro-mechanical approach can be followed, which has the potential to overcome the limitations of current phenomenological models. The discrete element (DE) method [3] is commonly applied for the study of granular materials under monotonic, static loads [12]. In this method, the equations of motion are solved for each particle, depending on the interaction with other particles. The contact law has a large influence on the constitutive behaviour of the sample. Since many microscopic properties are difficult to measure or model, simplifications are often made to the contact law. Linear models are mainly used for calculating the contact forces [1, 5]. Contact models based on the contact theories for elastic frictional contact, such as the theory of Hertz [9] for the normal component and Mindlin and Deresiewicz [11] for the tangential component, yield more realistic results. Hertz' contact theory is frequently used to compute the normal contact force [4, 6].

As the tangential contact force depends on the loading history of a contact, a linear incremental relation between the tangential displacement and the contact force is mostly applied. In order to incorporate the loading history, Walton and Braun [20] proposed a tangential contact model which is a simplification of the Mindlin-Deresiewicz contact theory, where several different loading histories are considered. Walton and Braun only distinguished between an increasing or decreasing tangential force. Vu-Quoc and Zhang [18] improved the model of Walton and Braun by considering 4 loading cases of the Mindlin-Deresiewicz theory for a varying normal contact force. The model of Walton and Braun is still applied when the normal force is constant.

A more realistic tangential contact model for elastic frictional contact is proposed [8], consisting of 16 loading cases which are based on 7 loading cases of the Mindlin-Deresiewicz contact theory. According to the contact theory, the model only makes use of scalar quantities. The three-dimensional (3D) implementation utilizes the framework by Vu-Quoc et al. [19]. Subsequently, numerical results of a triaxial test with the proposed contact model and a linear visco-elastic tangential contact model are compared.

The present study is a first step towards the development of a realistic micro-mechanical model of granular soils under repeated cyclic loading.

2 THE TANGENTIAL CONTACT MODEL

Hertz [9] studied the normal contact between elastic spheres. Starting from this theory, Mindlin and Deresiewicz [11] developed a contact theory for varying normal and tangential components of the contact forces. As the tangential component depends on the loading history, the theory is divided in a variety of loading cases. Based on the contact theory, an incremental solution is proposed, which is only valid when the increments in the normal ΔF_n and the tangential ΔF_t contact forces are small. In each loading case, the tangential contact force increment is given by:

$$\Delta F_\mathrm{t} = K_\mathrm{t}\, \Delta u_\mathrm{t}^\mathrm{rel} \tag{1}$$

where K_t is the tangential stiffness at the current time step, which incorporates the loading history, and $u_\mathrm{t}^\mathrm{rel}$ is the tangential component of the relative displacement between two contacting particles. The superscript 'rel' is omitted in the following as all displacements and velocities in this paper refer to the relative values between two particles in contact. The theory of Mindlin and Deresiewicz [11] is developed considering the stress distribution over the contact area between spherical particles. The distribution of the normal stress $\sigma_\mathrm{n}(\rho)$ over a circular contact area is given by Hertz' theory [9]:

$$\sigma_\mathrm{n}(\rho) = \frac{3F_\mathrm{n}}{2\pi a^3}\sqrt{a^2-\rho^2} \tag{2}$$

where a is the radius of the contact surface and ρ varies between 0 and a. This stress distribution results from the normal contact force F_n, which is related as follows to the relative normal displacement u_n of the two spheres:

$$F_\mathrm{n} = \frac{4\sqrt{R^\mathrm{eff}}E^\mathrm{eff}}{3}\,u_\mathrm{n}^{3/2} \tag{3}$$

where $1/R^\mathrm{eff} = (R_1+R_2)/(R_1R_2)$ is the relative contact curvature and E^eff is the effective elastic modulus, defined as:

$$E^\mathrm{eff} = \left(\frac{1-\nu_1^2}{E_1} + \frac{1-\nu_2^2}{E_2}\right)^{-1} \tag{4}$$

where ν_1 and ν_2 are the Poisson's ratios and E_1 and E_2 the Young's moduli of the two spheres in contact.

The distribution of the tangential stress τ, and thus the tangential contact force F_t, cannot be written in closed form as it depends on the loading history. Considering the case where the normal force is constant, the tangential force as a function of the relative tangential displacement u_t is given by a hysteresis curve shown in figure 1. The tangential stiffnesses, which relate the tangential force with the relative tangential displacement, are given by [11]:

$$K_\mathrm{t} = K_{\mathrm{t}0}\left(1-\frac{F_\mathrm{t}}{\mu F_\mathrm{n}}\right)^{1/3} \text{for } \dot{F}_\mathrm{t} > 0 \text{ and } |F_\mathrm{t}| \geq F_{\mathrm{t,max}}^\mathrm{tp} \text{ (curve 1)} \tag{5}$$

$$K_\mathrm{t} = K_{\mathrm{t}0}\left(1-\frac{F_\mathrm{t}^\mathrm{tp}-F_\mathrm{t}}{2\mu F_\mathrm{n}}\right)^{1/3} \text{for } \dot{F}_\mathrm{t} < 0 \text{ and } |F_\mathrm{t}| < F_{\mathrm{t,max}}^\mathrm{tp} \text{ (curve 2)} \tag{6}$$

$$K_\mathrm{t} = K_{\mathrm{t}0}\left(1-\frac{F_\mathrm{t}-F_\mathrm{t}^\mathrm{tp}}{2\mu F_\mathrm{n}}\right)^{1/3} \text{for } \dot{F}_\mathrm{t} > 0 \text{ and } |F_\mathrm{t}| < F_{\mathrm{t,max}}^\mathrm{tp} \text{ (curve 3)} \tag{7}$$

$$K_\mathrm{t} = K_{\mathrm{t}0}\left(1+\frac{F_\mathrm{t}}{\mu F_\mathrm{n}}\right)^{1/3} \text{for } \dot{F}_\mathrm{t} < 0 \text{ and } |F_\mathrm{t}| \geq F_{\mathrm{t,max}}^\mathrm{tp} \text{ (curve 4)} \tag{8}$$

Equations (5) to (8) show that the tangential stiffness depends on the normal contact force F_n, the tangential contact force F_t, the tangential contact force at the last turning

point $F_{\mathrm{t}}^{\mathrm{tp}}$, the maximal tangential force at a turning point $F_{\mathrm{t,max}}^{\mathrm{tp}}$, the coefficient of friction μ and the initial tangential stiffness K_{t0}:

$$K_{\mathrm{t0}} = 8a \left(\frac{2-\nu_1}{G_1} + \frac{2-\nu_2}{G_2} \right)^{-1} \tag{9}$$

where G_1 and G_2 are the shear moduli of the two contacting spheres. The maximal tangential force $F_{\mathrm{t,max}}^{\mathrm{tp}}$ is defined as the highest absolute value of the tangential force at a turning point occurred in the history of the contact.

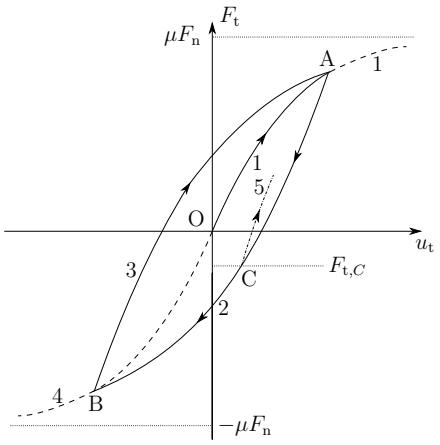

Figure 1: Tangential force F_{t} as a function of the tangential component u_{t} of the relative displacement for constant normal loading.

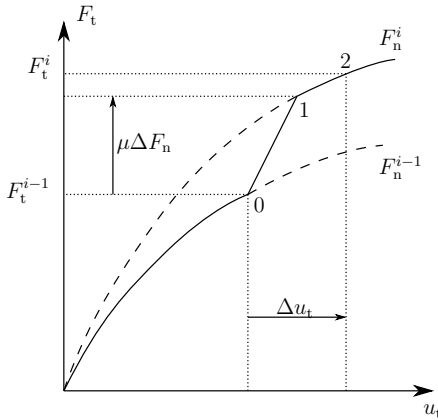

Figure 2: Tangential force F_{t} as a function of the relative tangential displacement u_{t} for increasing normal and tangential force, while $|F_{\mathrm{t}}^{i-1}| \geq F_{\mathrm{t,max}}^{\mathrm{tp}}$.

The case with a constant normal contact force occurs only in special configurations. The normal and tangential components of the contact force mostly vary arbitrarily. To account for this in DE calculations, equations (5) to (8) are approximated numerically, resulting into 16 loading cases [8] which depend on the loading history. The loading cases are divided in four main groups: (1) increasing normal force, increasing tangential force; (2) increasing normal force, decreasing tangential force; (3) decreasing normal force, increasing tangential force and (4) decreasing normal force, decreasing tangential force. These groups are based on the four loading cases defined by Vu-Quoc and Zhang [18], where the condition of an increasing/decreasing force is evaluated at the current time step.

In contradiction to the model of Vu-Quoc and Zhang, a distinction is made between the tangential force at the last turning point $F_{\mathrm{t}}^{\mathrm{tp}}$ and the maximal tangential force $F_{\mathrm{t,max}}^{\mathrm{tp}}$. In many cases, these parameters are equal, e.g. point A for curve 2 (figure 1). If point C is the last turning point (e.g. $F_{\mathrm{t}}^{\mathrm{tp}} = F_{\mathrm{t},C}$ on curve 5), the values of these parameters differ and a distinction is needed between $F_{\mathrm{t}}^{\mathrm{tp}}$ and $F_{\mathrm{t,max}}^{\mathrm{tp}}$ as the tangential stiffness depends on both. Four different loading situations can therefore be defined within each of the groups, cf. equations (5) to (8). These loading cases are defined based on the variation and value

of the tangential force at the previous time step $i-1$: (1) F_{t}^{i-1} increasing, $|F_{\mathrm{t}}^{i-1}| \geq F_{\mathrm{t,max}}^{\mathrm{tp}}$; (2) F_{t}^{i-1} decreasing, $|F_{\mathrm{t}}^{i-1}| < F_{\mathrm{t,max}}^{\mathrm{tp}}$; (3) F_{t}^{i-1} increasing, $|F_{\mathrm{t}}^{i-1}| < F_{\mathrm{t,max}}^{\mathrm{tp}}$ and (4) F_{t}^{i-1} decreasing, $|F_{\mathrm{t}}^{i-1}| \geq F_{\mathrm{t,max}}^{\mathrm{tp}}$.

The solution of Mindlin and Deresiewicz [11] is limited to simple loading histories, which are defined as a sequence of equilibrium positions. An equilibrium position is a state which can be achieved by holding the normal force constant at the current value and varying the tangential force. Every point on the curve of figure 1 corresponds to an equilibrium position for one specific value of the normal contact force.

In the following, as an example, the loading case of the first group (increasing normal force, increasing tangential force), where F_{t}^{i-1} is increasing and $|F_{\mathrm{t}}^{i-1}| \geq F_{\mathrm{t,max}}^{\mathrm{tp}}$, is discussed. An analogous procedure is used for the other 15 loading cases [8].

The loading case for F_{n}^{i}, F_{t}^{i} and F_{t}^{i-1} increasing and $|F_{\mathrm{t}}^{i-1}| \geq F_{\mathrm{t,max}}^{\mathrm{tp}}$

According to the Mindlin-Deresiewicz theory [11], the increment in the tangential contact force is achieved by first changing the normal force while the tangential force remains constant and then changing the tangential force under constant normal force. This means that first the normal force is increased to $F_{\mathrm{n}}^{i} = F_{\mathrm{n}}^{i-1} + \Delta F_{\mathrm{n}}$. The values of $F_{\mathrm{t}}^{\mathrm{tp}}$ and $F_{\mathrm{t,max}}^{\mathrm{tp}}$ are set to zero since this case corresponds to curve 1 in figure 1, where no turning point has yet occurred (figure 2). Then, under constant normal force, the tangential force is increased through a sequence of equilibrium positions ('simple loading history') until the final state is reached (figure 2, from state 0 to state 2). Two subcases are derived: $\Delta F_{\mathrm{t}} \geq \mu \Delta F_{\mathrm{n}}$ and $\Delta F_{\mathrm{t}} < \mu \Delta F_{\mathrm{n}}$. Since ΔF_{t} is unknown, these subcases are changed into [21] $\Delta u_{\mathrm{t}} \geq (\Delta u_{\mathrm{t}})_{01}$ and $\Delta u_{\mathrm{t}} < (\Delta u_{\mathrm{t}})_{01}$, where the displacement from state 0 to state 1 $(\Delta u_{\mathrm{t}})_{01} = \mu \Delta F_{\mathrm{n}} / (K_{\mathrm{t}})_{01}$. The tangential stiffness $(K_{\mathrm{t}})_{01}$ is taken constant and equal to the initial stiffness K_{t0} for a loading under constant normal force F_{n}^{i}. The latter is only true when the increment in the normal force ΔF_{n} is small.

When $\Delta u_{\mathrm{t}} \geq \mu \Delta F_{\mathrm{n}} / K_{\mathrm{t0}}$, as indicated in figure 2, the subsequent tangential force is given by:

$$F_{\mathrm{t}}^{i} = (F_{\mathrm{t}})_{1} + (K_{\mathrm{t}})_{12} (\Delta u_{\mathrm{t}})_{12} = F_{\mathrm{t}}^{i-1} + \mu \Delta F_{\mathrm{n}} + (K_{\mathrm{t}})_{12} \left(\Delta u_{\mathrm{t}} - \frac{\mu \Delta F_{\mathrm{n}}}{K_{\mathrm{t0}}} \right) \tag{10}$$

where the tangential stiffness $(K_{\mathrm{t}})_{12}$ is equal to (cf. equation (5)):

$$(K_{\mathrm{t}})_{12} = K_{\mathrm{t0}} \left(1 - \frac{F_{\mathrm{t}}^{i-1} + \mu \Delta F_{\mathrm{n}}}{\mu F_{\mathrm{n}}^{i}} \right)^{1/3} \tag{11}$$

When $\Delta u_{\mathrm{t}} < \mu \Delta F_{\mathrm{n}} / K_{\mathrm{t0}}$, the subsequent tangential force is given by:

$$F_{\mathrm{t}}^{i} = F_{\mathrm{t}}^{i-1} + K_{\mathrm{t0}} \, \Delta u_{\mathrm{t}} \tag{12}$$

However, the final state in equation (12) does not correspond to an equilibrium position, as it is not equivalent to a state of constant normal force and varying tangential force. The loading is therefore no longer part of a simple loading history. This causes inaccuracies, since the model is based on the assumption of simple loading histories.

3 IMPLEMENTATION IN 3D DISCRETE ELEMENT METHOD

To use the proposed tangential contact model in a 3D DE method requires vector manipulation since the model is only valid for a 2D model where the tangential plane at a contact point reduces to a line.

First, it is assumed that the orientation of the contact plane remains constant. In a 3D simulation, the direction of the tangential force in the tangential plane varies during the simulation. As a result, the above scalar model is not applicable. Nevertheless, the model can be applied in a 3D simulation if the components $\mathbf{F}_{\mathrm{t}\parallel}$ and $\mathbf{F}_{\mathrm{t}\perp}$ of the tangential force parallel and perpendicular to the initial relative tangential displacement increment $\Delta\mathbf{u}_{\mathrm{t}0}$ are considered [19]. The model is then applied in each direction separately. The direction of $\mathbf{F}_{\mathrm{t}\parallel}$ is equal to $\mathbf{t}_{\parallel} = -\Delta\mathbf{u}_{\mathrm{t}0}/||\Delta\mathbf{u}_{\mathrm{t}0}||$. The minus sign shows that the tangential force on a particle is opposite to the relative displacement of that particle.

After the directions of the tangential force components have been determined, the model proposed in the previous section can be applied. An increase or decrease in the tangential force $\mathbf{F}_{\mathrm{t}}$ is derived from the sign of the relative tangential displacement increment $\Delta\mathbf{u}_{\mathrm{t}}$, since the increment in each component $\Delta\mathbf{F}_{\mathrm{t}\parallel}$ and $\Delta\mathbf{F}_{\mathrm{t}\perp}$ of the tangential force is always opposite to the corresponding component $\Delta\mathbf{u}_{\mathrm{t}\parallel}$ and $\Delta\mathbf{u}_{\mathrm{t}\perp}$ of the relative tangential displacement increment (figure 3). For example, when $\Delta\mathbf{u}_{\mathrm{t}\parallel}$ is opposite to $\mathbf{t}_{\parallel}$, the components $\mathbf{u}_{\mathrm{t}\parallel}$ and $\mathbf{F}_{\mathrm{t}\parallel}$ of the relative tangential displacement and the tangential force parallel to the initial tangential displacement are increasing. The increment $\Delta F_{\mathrm{n}} = F_{\mathrm{n}}^{i} - F_{\mathrm{n}}^{i-1}$ in the normal force and the tangential force $\mathbf{F}_{\mathrm{t}\parallel}^{i-1}$ at the previous time step determine which loading case applies to the current time step. In the implementation of the model, the loading cases with a constant normal force are not considered, because the cases where the normal force is increasing converge towards the cases with a constant normal force.

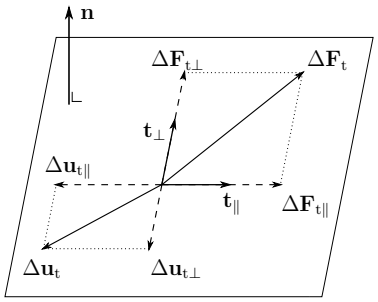

Figure 3: Positive increments of the relative tangential displacement and the tangential force shown in the tangential contact plane.

After application of the tangential model, the two components of the tangential force at the current time step i are known. These components, however, may not exceed the Coulomb friction limit, which determines the value of the tangential force in case of sliding: $|F_{\mathrm{t}\parallel}^{i}| \leq \mu F_{\mathrm{n}}^{i}$ and $|F_{\mathrm{t}\perp}^{i}| \leq \mu F_{\mathrm{n}}^{i}$.

So far, the directions and the values of the two components of the tangential force are calculated assuming the orientation of the tangential plane remains constant through the simulation. To account for the change in orientation of the contact plane, the direction of the components is corrected in each time step. The direction at the previous time step is projected onto the tangential contact plane at the current time step:

$$\mathbf{t}_{\parallel}^{i} = \mathbf{t}_{\parallel}^{i-1} - (\mathbf{t}_{\parallel}^{i-1} \cdot \mathbf{n}^{i})\mathbf{n}^{i} \tag{13}$$

$$\mathbf{t}_{\perp}^{i} = \mathbf{t}_{\perp}^{i-1} - (\mathbf{t}_{\perp}^{i-1} \cdot \mathbf{n}^{i})\mathbf{n}^{i} - (\mathbf{t}_{\perp}^{i-1} \cdot \mathbf{t}_{\parallel}^{i})\mathbf{t}_{\parallel}^{i} \tag{14}$$

where $\mathbf{n}^i$ is the unit normal vector of the tangential contact plane at time step i. This is less accurate than a rotation around the contact point, but acceptable since the force and displacement increments are small. The latter is a requirement of the tangential force-displacement model and inherent to the DE method. The third term in equation (14) ensures that $\mathbf{t}_{\perp}$ is always perpendicular to $\mathbf{t}_{\parallel}$.

Finally, the total tangential force in time step i is given by:

$$\mathbf{F}_{\mathrm{t}}^{i} = \mathbf{F}_{\mathrm{t}\parallel}^{i} + \mathbf{F}_{\mathrm{t}\perp}^{i} = F_{\mathrm{t}\parallel}^{i}\mathbf{t}_{\parallel}^{i} + F_{\mathrm{t}\perp}^{i}\mathbf{t}_{\perp}^{i} \tag{15}$$

Since this force has a larger value than each of its components, the Coulomb friction limit $|F_{\mathrm{t}}^{i}| \leq \mu F_{\mathrm{n}}^{i}$ is additionally enforced.

4 TRIAXIAL TEST SIMULATIONS

The proposed contact model is applied in the micro-mechanical simulation of a drained triaxial test and implemented in the DE software program *DEMeter++* [17].

The results are compared to results of a triaxial test simulation with a linear visco-elastic tangential contact model. The linear contact model is also applied incrementally:

$$\mathbf{F}_{\mathrm{t}}^{i} = \min\left(\mathbf{F}_{\mathrm{te}}^{i-1} - K_{\mathrm{lin}}\Delta\mathbf{u}_{\mathrm{t}} - A_{\mathrm{lin}}K_{\mathrm{lin}}\Delta\mathbf{v}_{\mathrm{t}}\,,\, \mu F_{\mathrm{n}}\frac{\mathbf{F}_{\mathrm{te}}^{i}}{||\mathbf{F}_{\mathrm{te}}^{i}||}\right) \tag{16}$$

where $\mathbf{F}_{\mathrm{te}}^{i-1}$ is the elastic part of the tangential force at the previous time step $i-1$, K_{lin} is a constant tangential stiffness, A_{lin} is a dissipative coefficient and $\mathbf{v}_{\mathrm{t}}$ is the relative velocity between two contacting spheres.

The normal contact force, in both simulations, is given by Hertz' theory (equation (3)), extended with a term to account for the dissipation of energy in every contact [14]:

$$F_{\mathrm{n}} = \frac{4E^{\mathrm{eff}}\sqrt{R^{\mathrm{eff}}}}{3}\left(u_{\mathrm{n}}^{3/2} + A_{\mathrm{n}}\sqrt{u_{\mathrm{n}}}\,v_{\mathrm{n}}\right) \tag{17}$$

where the dissipative coefficient is taken equal to $A_{\mathrm{n}} = 10^{-8}$ to ensure the stability of the calculations without affecting the results. This term is only added during the isotropic compression of the sample (section 4.1).

A soil sample with a diameter of 5 cm, a height of 12 cm and a mean particle diameter of 1 mm is used in the simulations. For a dense sand with a porosity $n = 0.35$, a huge

amount of particles are needed to simulate a full-scale triaxial test, which results in very high computation costs. Therefore, only a part of the soil sample is considered, indicated in figure 4a as a representative volume element (RVE). This RVE is much smaller than the soil sample, but large enough to give meaningful results.

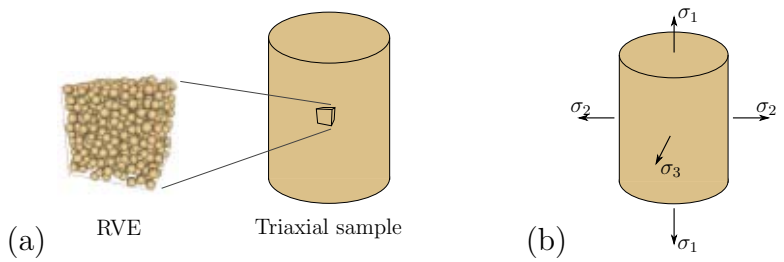

Figure 4: (a) Representative volume element (RVE) and (b) soil sample under triaxial conditions.

The simulation of a triaxial test is performed using a cubic RVE which contains 817 spherical particles. The micro-mechanical properties of the particles are based on the properties of quartz sand [16]: $E = 70\,\text{GPa}$, $\nu = 0.3$, density $\rho_\text{s} = 2650\,\text{kg/m}^3$ and friction coefficient $\mu = 0.3$. The parameters K_lin and A_lin for the linear contact model are found by calibrating the linear model to the proposed contact model. A poorly graded sand is used where the radii of the spheres follow a log-normal distribution with an average of 0.5 mm and a standard deviation of 0.05 mm. The minimum and maximum values for the radii are equal to 0.35 mm and 0.71 mm, respectively.

The RVE is modeled with periodic boundaries to represent the behaviour of the whole sample and avoid boundary effects. To control the deformation of the RVE the particles are subjected to a strain-rate tensor $\dot{\epsilon}_{ij}$ in addition to the displacements resulting from the interaction with other particles. A servo-control algorithm relates the strain-rate tensor to the stress tensor, which enables to follow stress-controlled loading paths [16]:

$$\left(\frac{\Delta\epsilon_{ij}}{\Delta t}\right)^i = \left(\frac{\Delta\epsilon_{ij}}{\Delta t}\right)^{i-1} + g\left(\sigma_{ij}^\text{d} - \sigma_{ij}^{i-1}\right) \tag{18}$$

where σ_{ij}^d is the target stress tensor, σ_{ij}^{i-1} is the calculated stress tensor at the previous time step and g is a gain parameter which value is obtained by trial and error [16]. A good value for g is found when the target stress path is followed correctly. The stress tensor is obtained as a volume average over all the contacts:

$$\sigma_{ij} = \frac{1}{V}\sum_{c=1}^{N_c} l_{ci}F_{cj} \tag{19}$$

where V is the volume of the RVE, N_c is the total amount of contacts, l_{ci} is the i-th component of the contact vector for contact c connecting two particles at their centers and F_{cj} is the j-th component of the contact force vector at that contact. Equation (18)

may be expressed in terms of individual or combinations of components of the strain-rate and stress tensors, depending on the loading path followed [16]. Since a triaxial test is a special case where the principal stresses σ_i are known (figure 4b), only these stresses are controlled by equation (18) and the corresponding strain rates $\dot{\epsilon}_i$ are applied to the particles to control the deformation of the RVE.

Due to the high Young's modulus, the critical time step is very small. The estimation of the critical time step [10] is based on an infinite series of point masses m connected with springs k. The smallest period, and thus the critical time step, occurs when the masses are moving in counter-phase, such that there is no motion at the center of each spring. A very small time step of $\Delta t = 10^{-7}\,\mathrm{s}$ is then obtained.

To allow for a larger time step, density-scaling is applied [16]: the density is scaled up by a factor $b = 10^{12}$. This results in an increase of the time step with a factor $\sqrt{b} = 10^6$, as the forces $\mathbf{F}$ and displacements $\mathbf{dx}$, which determine the stresses and strains, are not affected by the scaling. The accelerations $\mathbf{a}$ and velocities $\mathbf{v}$ are reduced by factors b and $\sqrt{b}$, respectively, but these quantities are not important when considering quasi-static behaviour. The following values for the density and time step are thus applied: $\rho_\mathrm{s} = 2650 \times 10^{12}\,\mathrm{kg/m^3}$ and $\Delta t = 0.1\,\mathrm{s}$.

4.1 Sample preparation

The RVE is created by random placement of the spherical particles, without overlapping, in a cubic volume with initial side length of 10 mm. The porosity is initially equal to $n = 0.55$. The sample is isotropically compressed to a mean normal stress $p = -100\,\mathrm{kPa}$, using principal strain rates, calculated with equation (18), with an initial value of $\dot{\epsilon}_1 = \dot{\epsilon}_2 = \dot{\epsilon}_3 = -10^{-4}/\mathrm{s}$, a maximal value of $|\dot{\epsilon}|_\mathrm{max} = 10^{-4}/\mathrm{s}$ and a gain parameter of $g = 10^{-7}$. In order to create a dense assembly, the friction coefficient is set to zero during the isotropic compression [16]. Prior to the triaxial test simulation, the friction coefficient is adjusted to $\mu = 0.3$. When applying the proposed tangential contact model, the porosity and mechanical average coordination number (amount of contacts per particle) after isotropic compression are $n = 0.3517$ and $Z_\mathrm{m} = 4.68$, respectively. When applying the linear contact model, the porosity and mechanical average coordination number after isotropic compression are $n = 0.3518$ and $Z_\mathrm{m} = 4.71$, respectively. This shows that the initial conditions for the two simulations are almost equal.

4.2 Triaxial test

A static triaxial test is performed by increasing the axial pressure σ_1 under constant confining stress $\sigma_2 = \sigma_3 = \sigma_c = -100\,\mathrm{kPa}$. The increase in the axial pressure is carried out in a strain controlled manner: a constant strain rate of $\dot{\epsilon}_1 = -10^{-5}\,/\mathrm{s}$ is applied vertically to the top and bottom of the RVE. The stresses σ_2 and σ_3 are held constant by applying the servo-control algorithm (equation (18)) with an initial value for the strain rates of $\dot{\epsilon}_2 = \dot{\epsilon}_3 = 0$ and a gain parameter of $g = 10^{-9}$.

The stress-strain behaviour for the simulation with the proposed tangential contact model is shown in figure 5 (black curve). A qualitative agreement with the theory of critical state soil mechanics [2, 15] is observed: yielding starts at a strain value of about 3%, after which a strain-softening and dilative behaviour is observed, converging to a constant deviatoric stress and volumetric strain. The critical state line is reached at about 30% axial strain.

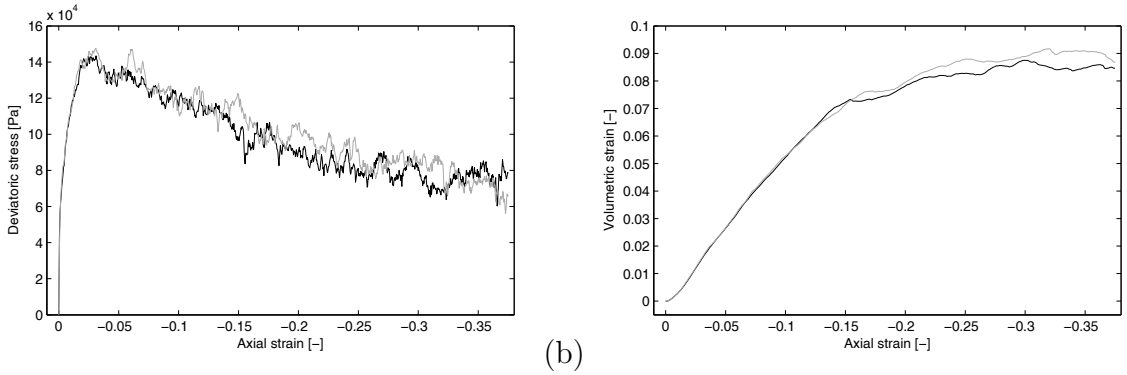

(a) (b)

Figure 5: Stress-strain behaviour of the triaxial test simulation with the proposed tangential contact model (black) and a calibrated linear tangential contact model (gray): (a) deviatoric stress and (b) volumetric strain as a function of the axial strain.

Calibration of the two simulations yields values of $K_{\text{lin}} = 10^5\,\text{N/m}$ and $A_{\text{lin}} = 1$ for the parameters of the linear contact model. With these values, the results of the two simulations are almost equal (figure 5). This illustrates that the stress-strain behaviour in a triaxial test is mainly governed by the normal contact model, which is the same in both simulations. The benefit of the proposed tangential contact model is that, while the parameters in the linear contact model have no physical meaning, it only makes use of physical properties of the particles, which are also used in the normal contact model (equation (17)): the Poisson's ratio ν, the Young's modulus E and the friction coefficient μ. The proposed model does not need calibration when the microscopic properties of the soil are known. The friction coefficient, however, is difficult to determine as it is function of the surface roughness of the particles. Nevertheless, the use of physical properties is expected to result in a more profound understanding of the behaviour of granular soils as insight is gained in the physical processes at micro-scale.

5 CONCLUSIONS

A tangential force-displacement model is proposed for elastic frictional contact between spherical particles, which is based on the theory by Mindlin and Deresiewicz [11]. The contact loading history is accounted for by considering 16 different loading cases. This results in an accurate evaluation of the tangential contact force. Since the model only makes use of scalar quantities, a 3D implementation of the model is given which requires vector

manipulation to keep track of the orientation of the tangential force and the evaluation of this force has to be done for each of its components separately.

A drained triaxial test on a dense sand is simulated, which is qualitatively in correspondence with the theory of critical state soil mechanics [2, 15]. The comparison of numerical results of a triaxial test obtained with the proposed and a linear tangential contact model shows the minor influence of the tangential contact force to the stress-strain behaviour compared to the normal contact force. The parameters of the proposed contact model have a physical meaning, which is expected to result in a more profound understanding of the micro-mechanical behaviour of granular soils.

REFERENCES

[1] N. Belheine, J.-P. Plassiard, F.-V. Donzé, F. Darve, and A. Seridi. Numerical simulation of drained triaxial test using 3D discrete element modeling. *Computers and Geotechnics*, 36:320–331, 2009.

[2] A.M. Britto and M.J. Gunn. *Critical soil state mechanics via finite elements*. Ellis Horwood Series in Civil Engineering. Ellis Horwood Ltd, 1987.

[3] P.A. Cundall and O.D.L. Strack. A discrete numerical model for granular assemblies. *Géotechnique*, 1:47–65, 1979.

[4] U. El Shamy and M. Zeghal. A micro-mechanical investigation of the dynamic response and liquefaction of saturated granular soils. *Soil Dynamics and Earthquake Engineering*, 27:712–729, 2007.

[5] A. Fakhimi. A hybrid discrete-finite element model for numerical simulation of geomaterials. *Computers and Geotechnics*, 36:386–395, 2009.

[6] S. Fazekas, J. Török, J. Kertész, and D.E. Wolf. Computer simulation of three dimensional shearing of granular materials: formation of shear bands. *Powders & Grains*, 5:223–226, 2005.

[7] S. François, C. Karg, W. Haegeman, and G. Degrande. A numerical model for foundation settlements due to deformation accumulation in granular soils under repeated small amplitude dynamic loading. *International Journal for Numerical and Analytical Methods in Geomechanics*, 34(3):273–296, 2010.

[8] P. Franken, S. François, and G. Degrande. A tangential force-displacement model for elastic frictional contact between discrete elements. Report BWM-2011-10, Department of Civil Engineering, K.U.Leuven, June 2011.

[9] H. Hertz. Über die Berührung fester elastischer Körper. *Journal für die reine und angewandte Mathematik*, 92:156–171, 1881.

[10] Itasca Consulting Group, Inc., Mineapolis, Minnesota. *PFC3D. Particle Flow Code in 3 Dimensions. User's guide.*, 2008.

[11] R.D. Mindlin and H. Deresiewicz. Elastic spheres in contact under varying oblique forces. *Journal of Applied Mechanics, Transactions of the ASME*, pages 327–344, 1953.

[12] F. Nicot and F. Darve. Micro-mechanical bases of some salient constitutive features of granular materials. *International Journal of Solids and Structures*, 44:7420–7443, 2007.

[13] A. Niemunis, T. Wichtmann, and T. Triantafyllidis. A high-cycle accumulation model for sand. *Computers and Geotechnics*, 32:245–263, 2005.

[14] T. Pöschel and T. Schwager. *Computational Granular Dynamics: Models and Algorithms*. Springer, 2005.

[15] A. N. Schofield and C. P. Wroth. *Critical state soil Mechanics*. McGraw-Hil, 1968.

[16] C. Thornton. Numerical simulations of deviatoric shear deformation of granular media. *Géotechnique*, 50:43–53, 2000.

[17] E. Tijskens, H. Ramon, and J. De Baerdemaeker. Discrete element modelling for process simulation in agriculture. *Journal of Sound and Vibration*, 266:493–514, 2003.

[18] L. Vu-Quoc and X. Zhang. An accurate and efficient tangential force-displacement model for elastic frictional contact in particle-flow simulations. *Mechanics of Materials*, 31:235–269, 1999.

[19] L. Vu-Quoc, X. Zhang, and O.R. Walton. A 3-D discrete-element method for dry granular flows of ellipsoidal particles. *Computer Methods in Applied Mechanics and Engineering*, 187:483–528, 2000.

[20] O.R. Walton and R.L. Braun. Viscosity, granular-temperature, and stress calculations for shearing assemblies of inelastic, frictional disks. *Journal of Rheology*, 30:949–980, 1986.

[21] X. Zhang and L. Vu-Quoc. An accurate elasto-plastic frictional tangential force-displacement model for granular-flow simulations: Displacement-driven formulation. *Journal of Computational Physics*, 225:730–752, 2007.